J Sol-Gel Sci Technol (2015) 75:664–669
DOI 10.1007/s10971-015-3736-y

ORIGINAL PAPER

Preparation and light-controlled resistive switching memory behavior of $CuCr_2O_4$

Bai Sun[1,2] · Jianhong Wu[1] · Xiangjiang Jia[1] · Fangming Lou[2] · Peng Chen[1]

Received: 7 October 2014 / Accepted: 9 May 2015 / Published online: 16 May 2015

Abstract In this work, $CuCr_2O_4$ nanoparticles were successfully prepared by an improved hydrothermal process, and a resistive switching memory behavior with Ag/$CuCr_2O_4$/fluorine-doped tin oxide structure is demonstrated. Specially, the resistive switching memory characteristics can be controlled by white-light illumination. The device can maintain superior stability over 100 cycles with an OFF/ON-state resistance ratio of about 10^3 at room temperature. This study is useful for exploring the promising light-controlled resistive switching memory device in the development of resistive switching random-access memory.

Graphical Abstract We demonstrate a resistive switching device based on Ag/$CuCr_2O_4$/FTO structure, and the device shows light-controlled resistive switching memory characteristics.

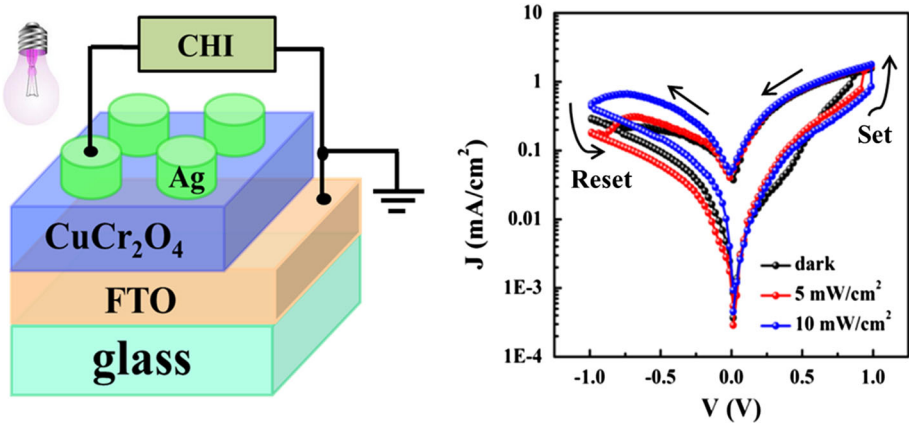

Keywords $CuCr_2O_4$ · Hydrothermal method · Resistive switching · White light · Memory device

1 Introduction

The resistive switching phenomenon basing on the electrical-pulse-regulated resistance in a metal–insulator–metal sandwich structure has recently attracted a great deal of attention due to potential application for nonvolatile random-access memory [1–6]. So far, the resistive switching phenomenon, in which the resistance can be switched

✉ Peng Chen
pchen@swu.edu.cn

[1] School of Physics Science and Technology, Southwest University, Chongqing 400715, China

[2] Institute for Clean Energy and Advanced Materials (ICEAM), Southwest University, Chongqing 400715, China

between a high resistance state (HRS) and a low resistance state (LRS) by electrical pulse, has been observed in many semiconducting and insulating materials including binary transition metal oxides [7–11], perovskite oxides [12–14], chalcogenides [15, 16], sulfides [17], amorphous silicon [18], organic materials [19, 20], and ferroelectric materials [21, 22]. Accordingly, various models have been suggested to explain the resistive switching phenomenon, including the metal–insulator phase transition [14, 23], the ferroelectric polarization [24–26], the conductive bridge constructed by the migration of localized metal atoms or defects [11, 27], and the formation and elimination of conductive pathways induced by the external electric field [28]. However, the resistive switching mechanisms are still being debated [1, 2].

In past few years, nanoscale transition metal oxides and composites significantly exhibit enhanced physical, chemical, electrical, optical, or magnetic properties, which lead to extensive applications in electronic device, electrochemistry, biomedical device, and other fields [29–33]. Copper–chromium oxide $CuCr_2O_4$ often acts as numerous oxidation, hydrogenation, decomposition of alcohols and alkylation reactions, and so on [34]. On the other hand, $CuCr_2O_4$, a p-type semiconductor with narrow band gap, is a versatile catalyst due to its stable structure [35]. $CuCr_2O_4$ has been reported as an efficient catalyst for various chemical processes such as oxidation, hydrogenation, dehydrogenation, dehydrocyclization, hydrogen production, and decomposition of organic compounds [36, 37]. Therefore, the applications of $CuGr_2O_4$ are particularly extensive.

Although there are a large number of reports on various applications of $CuCr_2O_4$ in previous works, the resistive switching properties of $CuCr_2O_4$ have not been reported so far. Herein, we report resistive switching behavior of Ag/$CuCr_2O_4$/FTO device. Specially, the resistive switching characteristics of Ag/$CuCr_2O_4$/FTO device can be controlled by white light.

2 Experimental procedures

2.1 Preparation of $CuCr_2O_4$ nanoparticles

The $CuCr_2O_4$ spinel nanoparticles were prepared by an improved hydrothermal process using cetyltrimethylammonium bromide (CTAB) as the surfactant, which is similar to the methods suggested in previous works [38, 39]. All the chemicals used in this work were of analytical grade and used directly without further purification. The distilled water was used as a solvent throughout the experiments. First, $Cu(NO_3)_2{\cdot}2.5H_2O$ (3.2 g) and $Cr(NO_3)_3{\cdot}9H_2O$ (8.0 g) were dissolved in 200 ml distilled water with stirring. Then 200 ml of solution with $(CH_2)_6N_4$ of 0.01 mol and NH_4HCO_3 of 0.1 mol was added into above solution. After stirring continuously for 2 h, the precipitate was filtered and washed with distilled water and ethanol for several times until the pH value was 6.5–7.5. Second, the co-precipitate was redispersed in 80 ml of distilled water under vigorous stirring for 30 min. Then 0.5 g cationic surfactant cetyltrimethylammonium bromide (CTAB) was added into above solution under stirring. Then the solution was transferred to a 100-ml sealed Teflon-lined steel autoclave. And the sealed Teflon-lined steel autoclave was heated at 180 °C for 24 h. After the autoclave was cooled to room temperature, the powder obtained was washed with distilled water and ethanol and dried at 60 °C for 12 h. Finally, we annealed the as-prepared $CuCr_2O_4$ powder at 900 °C in air for 2 h with a gradual heating rate of 10 °C min^{-1}.

2.2 Preparation of Ag/$CuCr_2O_4$/FTO device

First, fluorine-doped tin oxide (FTO) substrates were cleaned by acetone, ethanol, and deionized water and subsequently dried on the spin coater. Second, $CuCr_2O_4$ films were prepared on FTO substrate by spin-coating method. The detailed preparation process of $CuCr_2O_4$ films is as follows: First, we grinded the as-prepared powder for 2 h. Next, we dissolved the powder in toluene solution to prepare precursor gel. Then the precursor gel was spin-coated on the FTO substrate. The spin-coating process at 5000 rpm for 10 s was used for film deposition. Second, these samples were subsequently dried at 60 °C in vacuum for overnight. The thickness of the films was detected by the step profiler.

2.3 Characterizations

Crystal structure of $CuCr_2O_4$ film was characterized at room temperature by X-ray diffraction (XRD) with Cu $K\alpha$ radiation. The microstructure of the $CuCr_2O_4$ film was observed by transmission electron microscopy. In the test of resistive switching characterizations, Ag is top electrode and FTO is bottom electrode. Ag electrodes were prepared by vacuum deposition. And the preparation process of Ag electrodes is as follows: First, we covered surface of $CuCr_2O_4$/FTO with a mask. Second, we put it into the vacuum sputtering system to grow Ag electrodes. Finally, we chose the superior electrodes for characterization. Current density–voltage (J–V) and resistance–cycle curves were tested using the electrochemical workstation at room temperature. We used an ordinary filament lamp with various power densities as light source. The wavelength range of light is 400–760 nm.

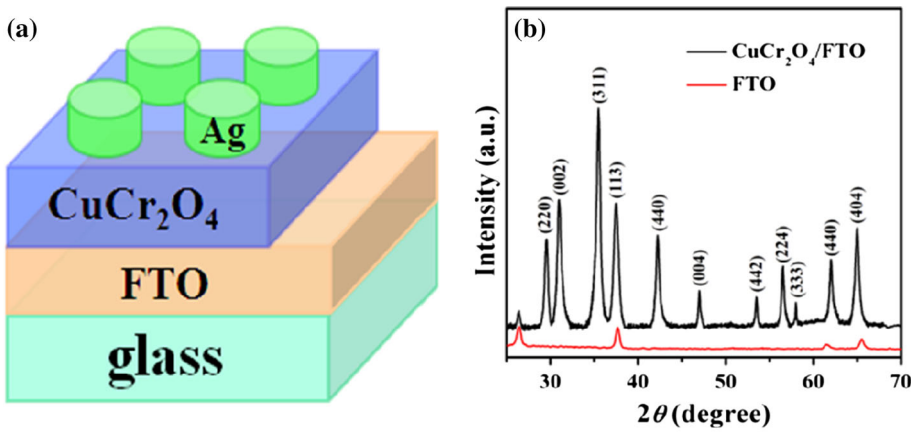

Fig. 1 **a** Schematic representation of the device. **b** The X-ray diffraction (XRD) of $CuCr_2O_4$/FTO structure and FTO substrate

3 Results and discussion

Figure 1a shows the schematic representation of the device, where the $CuCr_2O_4$ film was spin-coated on the FTO substrate, and the electrodes of Ag with the area were deposited onto the $CuCr_2O_4$ film. The crystalline structure of the samples was characterized by XRD patterns. Figure 1b displays the XRD of $CuCr_2O_4$/FTO structure. The peaks of FTO substrate are obvious (Fig. 1b). In order to make diffraction peaks of $CuCr_2O_4$ film more clear, we also present the XRD pattern of the pure FTO substrate without $CuCr_2O_4$ film in Fig. 1b. Figure 1b exhibits the XRD pattern of $CuCr_2O_4$/FTO. We can see there are only the peaks of $CuCr_2O_4$ besides peaks of FTO substrate. The diffraction patterns in Fig. 1b agree with tetragonal $CuCr_2O_4$ with spinel structure [38–40]. The XRD demonstrates the characteristic diffraction peaks of $CuCr_2O_4$ with spinel structure, which is in good agreement with JCPDS-No 34-0424 [38]. No characteristic diffraction peaks owing to CuO and Cr_2O_3 are detected. Therefore, the films contain only pure $CuCr_2O_4$, and the sharp peaks demonstrate good crystallinity of the $CuCr_2O_4$.

Figure 2a presents the high-resolution transmission electron microscope (HRTEM) image of $CuCr_2O_4$ film. The fringes with a spacing of 0.27 nm correspond to (311) planes of $CuCr_2O_4$, which indicates that the $CuCr_2O_4$ film is single-crystalline structure for individual $CuCr_2O_4$ nanoparticle. The composition of $CuCr_2O_4$ film is further confirmed by elemental analysis carried out from energy-dispersive X-ray spectra (EDX). The EDX data in Fig. 2b confirm that the compositions of the film are Cu, Cr, and O without any other impurities. And the atomic percentage Cu/Cr/O of $CuCr_2O_4$ film is about 1:2:4 from the inset of Fig. 2b.

Figure 3 displays the UV–Vis absorption spectrum of $CuCr_2O_4$ nanoparticles without FTO substrate. The onset of the absorption located at about 580 nm indicates that as-prepared $CuCr_2O_4$ nanoparticles have good light absorption properties in the visible light region.

In order to obtain the resistive switching characteristics of Ag/$CuCr_2O_4$/FTO structure under white-light illumination with various power densities, we employed the experimental test circuit shown in inset of Fig. 4a. Figure 4a displays the current density–voltage (J–V) characteristic curves of Ag/$CuCr_2O_4$/FTO device in linear scale under illumination with various power densities, which exhibits an asymmetric behavior with significant hysteresis. The

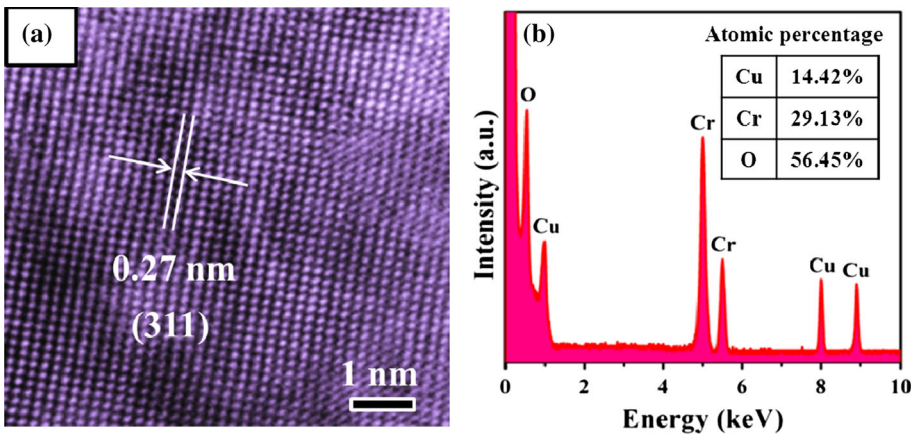

Fig. 2 **a** High-resolution transmission electron microscope (HRTEM) image of $CuCr_2O_4$ film. **b** The energy-dispersive X-ray (EDX) spectrum of $CuCr_2O_4$ film; the *inset* shows that the atomic percentage of $CuCr_2O_4$ film is about 1:2:4

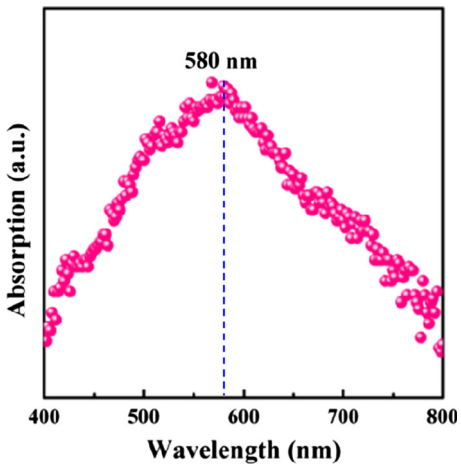

Fig. 3 PL behavior of $CuCr_2O_4$ powders at room temperature

arrows in the figure denote the sweeping direction of voltage. We found that the response time is about 0.1–0.2 s.

Figure 4b shows a corresponding J–V curve of Ag/$CuCr_2O_4$/FTO device in logarithmic scale with resistance switching effects. The arrows in Fig. 4b denote the sweeping direction of voltage. We can see that a sudden current increase occurs at about 0.85 V (V_{Set}) in the dark and about 0.9 V (V_{Set}) under white-light illumination with power density of 5 mW/cm^2, indicating a resistive switching from the high resistance state (HRS or "OFF") to the low resistance state (LRS or "ON"), which was called the "Set" process. With further increasing the power density to 10 mW/cm^2, the V_{Set} reaches to 0.98 V. When the applied voltage sweeps from zero to negative voltage of about −0.75 V (V_{Reset}) in the dark and −0.98 V under white-light illumination with power density 10 mW/cm^2, the device can return to the HRS, which was called the "Reset" process. During the successive "Set" and "Reset" cycles on the same device, the device shows the identical J–V curves. The V_{Reset} and V_{Set} are almost unchanged in subsequent cycles. The threshold voltages in the device are ≤1.0 V, which is an attractive advantage for practical memory applications in an expansive condition [41, 42].

Figure 5a displays the evolutions of V_{Set} and V_{Reset} over 100 successive resistive switching cycles on the device. We find that there is only little fatigue for switching voltages V_{Set} and V_{Reset}. The V_{Set} and V_{Reset} are 0.75 ± 0.06 V and −0.7 ± 0.1 V, respectively, in the dark, and the V_{Set} and V_{Reset} are increased to 0.92 ± 0.08 V and −0.9 ± 0.1 V, respectively, under white-light illumination with power density of 10 mW/cm^2, indicating low fatigue for switching voltages of the Ag/$CuCr_2O_4$/FTO structure, which reflects excellent switching stability of V_{Set} and V_{Reset} to a certain extent. It is worth noting that the illumination can control the switching voltage V_{Set} and V_{Reset}. The absolute values of V_{Reset} and V_{Set} increase with the increasing power density of illumination. That is to say that the illumination can control the resistive switching, which is consistent with the reported results in previous literature [43–47].

To estimate the probably practicability of white-light-controlled resistive switching behaviors of the Ag/$CuCr_2O_4$/FTO structure device, the resistance–cycle number curve for the HRS and LRS with a positive bias of 0.1 V is tested and shown in Fig. 5b. It is obvious that the resistances are about 1.1 KΩ at the LRS (ON state) and 2.5 MΩ at the HRS (OFF state) in the dark, and the resistances are about 1.05 KΩ at the LRS (ON state) and 2.48 MΩ at the HRS (OFF state) under illumination with power density of 10 mW/cm^2. The OFF/ON-state resistance ratio is up to 10^3. Both the LRS resistance and the HRS resistance decrease with the increasing power density of illumination. According to the above results, the steady white-light-controlled resistive switching behavior in Ag/$CuCr_2O_4$/FTO structure with an OFF/ON-state resistance ratio of about 10^3 provides the potential for light-controlled non-volatile memory applications.

The mechanism for resistive switching in a metal/oxides/metal structure has been extensively investigated, but

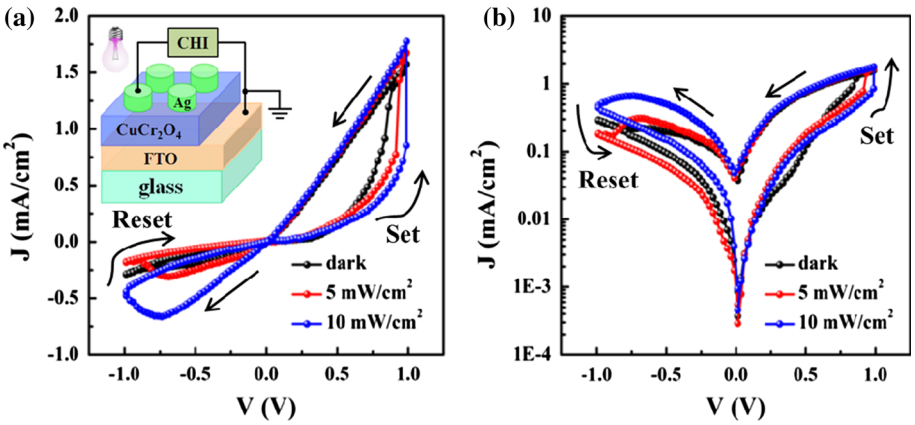

Fig. 4 **a** Current density–voltage (J–V) characteristic curves in linear scale of Ag/$CuCr_2O_4$/FTO structure in the dark and under white-light illumination with various power densities; the *inset* presents the real test circuit. **b** The corresponding J–V characteristic curves in logarithmic scale

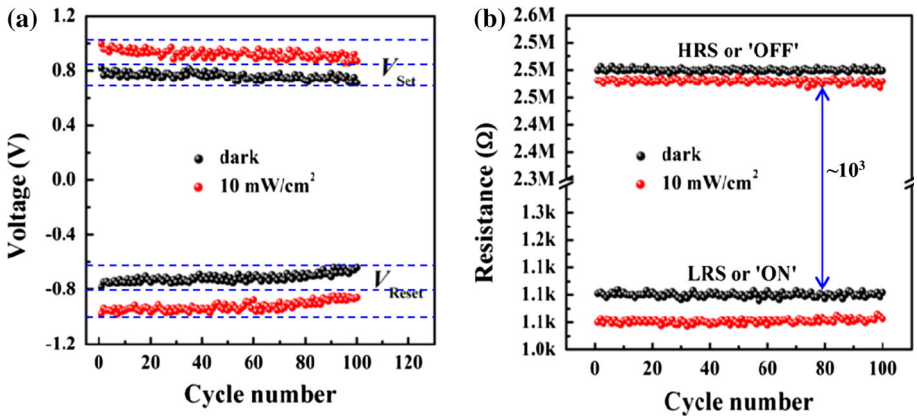

Fig. 5 **a** Evolution of switching voltages including V_{Set} and V_{Reset} during the 100 resistive switching cycles in the dark and under light illumination with power density 10 mW/cm^2. **b** The resistance–cycle curve with a positive bias voltage of 0.1 V in the dark and under light illumination with power density 10 mW/cm^2

is still controversial [34, 44]. In our works, the asymmetric behavior of J–V curve indicates that a Schottky barrier is formed at the interfaces of Ag/$CuCr_2O_4$ and $CuCr_2O_4$/FTO. This bipolar resistive switching behavior should be resulted from the trapped and detrapped charge in the Schottky-like depletion layer [48–54]. The white light can modulate the resistive switching behavior by a large number of photogenerated charges [44–47].

4 Conclusions

In brief, the reversible bipolar resistive switching characteristics of Ag/$CuCr_2O_4$/FTO device are observed. In particularly, the white light can control the resistance switching behavior. Therefore, the superior resistance switching characteristics of the Ag/$CuCr_2O_4$/FTO device hold a great promise for next-generation nonvolatile light-controlled memory applications.

Acknowledgments This work was supported by the National Science Foundation of China (Grant No. 51372209).

References

1. Waser R, Aono M (2007) Nanoionics-based resistive switching memories. Nat Mater 6:833–840
2. Yang JJ, Pickett MD, Li XM, Ohlberg DAA, Stewart DR, Williams RS (2008) Memristive switching mechanism for metal/oxide/metal nanodevices. Nat Nanotechnol 3:429–433
3. Chanthbouala A, Garcia V, Cherifi RO, Bouzehouane K, Fusil S, Moya X, Xavier S, Yamada H, Deranlot C, Mathur ND, Bibes M, Barthélémy A, Grollier J (2012) A ferroelectric memristor. Nat Mater 11:860–864
4. Xu XY, Yin ZY, Xu CX, Dai J, Hu JG (2014) Resistive switching memories in MoS_2 nanosphere assemblies. Appl Phys Lett 104:033504
5. Sun B, Li QL, Liu YH, Chen P (2015) Resistive switching of multiferroic $BiCoO_3$ nanoflowers. Funct Mater Lett 8:1550001
6. Sun B, Li CM (2014) Superior resistive switching behaviors of $FeWO_4$ single-crystalline nanowires array. Chem Phys Lett 604:127–130
7. Nagashima K, Yanagida T, Oka K, Taniguchi M, Kawai T, Kim JS, Park BH (2010) Resistive switching multistate nonvolatile memory effects in a single cobalt oxide nanowire. Nano Lett 10:1359–1363
8. Qi J, Olmedo M, Ren J, Zhan N, Zhao J, Zheng JG, Liu JL (2012) Resistive switching in single epitaxial ZnO nanoislands. ACS Nano 6:1051–1058
9. He L, Liao ZM, Wu HC, Tian XX, Xu DS, Cross GLW, Duesberg GS, Shvets IV, Yu DP (2011) Memory and threshold resistance switching in Ni/NiO core–shell nanowires. Nano Lett 11:4601–4606
10. Sun B, Li HW, Wei LJ, Chen P (2014) Hydrothermal synthesis and resistive switching behaviour of WO_3/$CoWO_4$ core–shell nanowires. CrystEngComm 16:9891–9895
11. Sun B, Liu YH, Zhao WX, Wu JG, Chen P (2015) Hydrothermal preparation and white-light-controlled resistive switching behavior of $BaWO_4$ nanospheres. Nano Micro Lett 7:80–85
12. Szot K, Speier W, Bihlmayer G, Waser R (2006) Switching the electrical resistance of individual dislocations in single-crystalline $SrTiO_3$. Nat Mater 5:312–320
13. Asamitsu A, Tomioka Y, Kuwahara H, Tokura Y (1997) Current switching of resistive states in magnetoresistive manganites. Nature 388:50–52
14. Kim DS, Kim YH, Lee CE, Kim YT (2006) Colossal electroresistance mechanism in a Au/$Pr_{0.7}Ca_{0.3}MnO_3$/Pt sandwich structure: evidence for a Mott transition. Phys Rev B 74:174430
15. Wuttig M (2005) Phase-change materials—towards a universal memory? Nat Mater 4:265–266
16. Li Y, Zhong YP, Xu L, Zhang JJ, Xu XH, Sun HJ, Miao XS (2013) Ultrafast synaptic events in a chalcogenide memristor. Sci Rep 3:1619
17. Liao ZM, Hou C, Zhao Q, Wang DS, Li YD, Yu DP (2009) Resistive switching and metallic-filament formation in Ag_2S nanowire transistors. Small 5:2377–2381
18. Jo SH, Kim KH, Lu W (2009) High-density crossbar arrays based on a Si memristive system. Nano Lett 9:870–874
19. Lee T, Chen Y (2012) Organic resistive nonvolatile memory materials. MRS Bull 37:144–149
20. Liu ZM, Yasseri AA, Lindsey JS, Bocian DF (2003) Molecular memories that survive silicon device processing and real-world operation. Science 302:1543–1545
21. Yan F, Xing GZ, Li L (2014) Low temperature dependent ferroelectric resistive switching in epitaxial $BiFeO_3$ films. Appl Phys Lett 104:132904
22. Lin YB, Yan ZB, Lu XB, Lu ZX, Zeng M, Chen Y, Gao XS, Wan JG, Dai JY, Liu JM (2014) Temperature-dependent and polarization-tuned resistive switching in Au/$BiFeO_3$/$SrRuO_3$ junctions. Appl Phys Lett 104:143503

23. Rozenberg MJ, Inoue IH, Sanchez MJ (2006) Strong electron correlation effects in nonvolatile electronic memory devices. Appl Phys Lett 88:033510
24. Tsymbal EY, Kohlstedt H (2006) Applied physics—tunneling across a ferroelectric. Science 313:181–183
25. Kohlstedt H, Pertsev NA, Contreras JR, Waser R (2005) Theoretical current–voltage characteristics of ferroelectric tunnel junctions. Phys Rev B 72:125341
26. Sun B, Li CM (2015) Light-controlled resistive switching memory of multiferroic $BiMnO_3$ nanowires array. Phys Chem Chem Phys 17:6718–6721
27. Lee D, Seong D, Jo I, Xiang F, Dong R, Oh S, Hwang H (2007) Resistance switching of copper doped MoO_x films for nonvolatile memory applications. Appl Phys Lett 90:122104
28. Wang LH, Yang W, Sun QQ, Zhou P, Lu HL, Ding SJ, Zhang DW (2012) The mechanism of the asymmetric SET and RESET speed of graphene oxide based flexible resistive switching memories. Appl Phys Lett 100:063509
29. Xiao HM, Zhu LP, Liu XM, Fu SY (2007) Anomalous ferromagnetic behavior of CuO nanorods synthesized via hydrothermal method. Solid State Commun 141:431–435
30. Waghulade RB, Patil PP, Pasricha R (2007) Synthesis and LPG sensing properties of nano-sized cadmium oxide. Talanta 72:594–599
31. Valdés-Solís T, Marbán G, Fuertes AB (2006) Nanosized catalysts for the production of hydrogen by methanol steam reforming. Catal Today 116:354–360
32. Duque JGS, Souza EA, Meneses CT, Kubota L (2007) Magnetic properties of $NiFe_2O_4$ nanoparticles produced by a new chemical method. Phys B 398:287–290
33. Cui H, Zayat M, Levy D (2005) Sol-gel synthesis of nanoscaled spinels using propylene oxide as a gelation agent. J Sol Gel Sci Technol 35:175–181
34. Kawamoto AM, Pardini LC, Rezende LC (2004) Synthesis of copper chromite catalyst. Aerosp Sci Technol 8:591–598
35. Bajaj R, Sharma M, Bahadur D (2013) Visible light-driven novel nanocomposite ($BiVO_4/CuCr_2O_4$) for efficient degradation of organic dye. Dalton Trans 42:6736–6744
36. Yan J, Zhang L, Yang H, Tang Y, Lu Z, Guo S, Dai Y, Han Y, Yao M (2009) $CuCr_2O_4/TiO_2$ heterojunction for photocatalytic H-2 evolution under simulated sunlight irradiation. Sol Energy 83:1534–1539
37. Boumaza S, Bouarab R, Trari M, Bouguelia A (2009) Hydrogen photo-evolution over the spinel $CuCr_2O_4$. Energy Convers Manage 50:62–68
38. Pan L, Li L, Bao X, Chen Y (2012) Highly photocatalytic activity for p-nitrophenol degradation with spinel-structured $CuCr_2O_4$. Micro Nano Lett 7:415–418
39. Acharyya SS, Ghosh S, Tiwari R, Sarkar B, Singha RK, Pendem C, Sasaki T, Bal R (2014) Preparation of the $CuCr_2O_4$ spinel nanoparticles catalyst for selective oxidation of toluene to benzaldehyde. Green Chem 16:2500–2508
40. Zhang P, Shi Y, Chi M, Park JN, Stucky GD, McFarland EW, Gao L (2013) Mesoporous delafossite $CuCrO_2$ and spinel $CuCr_2O_4$: synthesis and catalysis. Nanotechnology 24:345704
41. Dong H, Zhang X, Zhao D, Niu Z, Zeng Q, Li J, Cai L, Wang Y, Zhou W, Gaob M, Xie S (2012) High performance bipolar resistive switching memory devices based on Zn_2SnO_4 nanowires. Nanoscale 4:2571–2574
42. Yang Y, Zhang X, Gao M, Zeng F, Zhou W, Xie S, Pan F (2011) Nonvolatile resistive switching in single crystalline ZnO nanowires. Nanoscale 3:1917–1921
43. Ungureanu M, Zazpe R, Golmar F, Stoliar P, Llopis R, Casanova F, Hueso LE (2012) A light-controlled resistive switching memory. Adv Mater 24:2496–2500
44. Choi DH, Lee D, Sim H, Chang M, Hwang HS (2006) Reversible resistive switching of $SrTiO_x$ thin films for nonvolatile memory applications. Appl Phys Lett 88:082904
45. Park J, Lee S, Lee J, Yong K (2013) A light incident angle switchable ZnO nanorod memristor: reversible switching behavior between two non-volatile memory devices. Adv Mater 25:6423–6429
46. Park J, Lee S, Yong K (2012) Photo-stimulated resistive switching of ZnO nanorods. Nanotechnology 23:385707
47. Sun B, Liu YH, Zhao WX, Chen P (2015) Magnetic-field and white-light controlled resistive switching behaviors in Ag/$[BiFeO_3/\gamma\text{-}Fe_2O_3]$/FTO device. RSC Adv 5:13513–13518
48. Deng XL, Hong S, Hwang I, Kim JS, Jeon JH, Park YC, Lee J, Kang SO, Kawai T, Park BH (2012) Confining grains of textured Cu_2O films to single-crystal nanowires and resultant change in resistive switching characteristics. Nanoscale 4:2029–2033
49. Chen XG, Fu JB, Liu SQ, Yang YB, Wang CS, Du HL, Xiong GC, Lian GJ, Lian GJ, Yang JB (2012) Trap-assisted tunneling resistance switching effect in $CeO_2/La_{-0.7}(Sr_{0.1}Ca_{0.9})_{0.3}MnO_3$ heterostructure. Appl Phys Lett 101:153509
50. Chen XG, Ma XB, Yang YB, Chen LP, Xiong GC, Lian GJ, Yang YC, Yang JB (2011) Comprehensive study of the resistance switching in $SrTiO_3$ and Nb-doped $SrTiO_3$. Appl Phys Lett 98:122102
51. Rubi D, Gomez-Marlasca F, Bonville P, Colson D, Levy P (2012) Resistive switching in ceramic multiferroic $Bi_{0.9}Ca_{0.1}FeO_3$. Phys B 407:3144–3146
52. Sawa A, Fujii T, Kawasaki M, Tokura Y (2004) Hysteretic current-voltage characteristics and resistance switching at a rectifying $Ti/Pr_{0.7}Ca_{0.3}MnO_3$ interface. Appl Phys Lett 85:4073–4075
53. Zazpe R, Ungureanu M, Golmar F, Stoliar P, Llopis R, Casanova F, Pickup DF, Rogerofh C, Hueso LE (2014) Resistive switching dependence on atomic layer deposition parameters in HfO_2-based memory devices. J Mater Chem C 2:3204–3211
54. Lin CY, Lee DY, Wang SY, Lin CC, Tseng TY (2008) Effect of thermal treatment on resistive switching characteristics in Pt/Ti/Al_2O_3/Pt devices. Surf Coat Technol 203:628–631